JOURNAL OF MATERIALS SCIENCE **38** (2003) 207–215

Tensile deformation mechanism of polyamide 6,6/SEBS-g-MA blend and its hybrid composites reinforced with short glass fibers

SIE CHIN TJONG*
Department of Physics and Materials Science, City University of Hong Kong, Tat Chee Avenue, Kowloon, Hong Kong, People's Republic of China
E-mail: aptjong@cityu.edu.hk

SHI-AI XU
Institute of Polymer Science and Engineering, East China University of Science and Technology, 130 Mei Long Road, Shanghai 200237, People's Republic of China

YIU-WING MAI
MEEM Department, City University of Hong Kong, Hong Kong, People's Republic of China; School of Aerospace, Mechanical and Mechatronic Engineering, The University of Sydney, Sydney, Australia

Short glass fiber (SGF) reinforced polyamide 6,6 hybrid composites toughened with maleated styrene-ethylene butylenes-styrene (SEBS-g-MA) elastomer were prepared by compounding and subsequent injection molding. The hybrids were reinforced with 5, 10, 15, 20 and 30 wt% SGF. The matrix of the hybrids consisted of 80 wt% PA6,6 and 20 wt% SEBS-g-MA. Dilatometery was employed to characterize the deformation mechanisms of tough PA6,6/SEBS-g-MA 80/20 blend and its hybrid composites under uniaxial tension. Dilatometric responses showed that both cavitation and shear yielding occur in PA6,6/SEBS-g-MA 80/20 blend during deformation. And the cavitation deformation prevailed over shear yielding in this blend after the initial elastic deformation. Moreover, the volume strain was observed to increase considerably with increasing SGF content for the hybrids investigated. SEM examination revealed that microvoids originated from the debonding of glass fiber from the PA6,6 matrix were responsible for the cavitation strain in the hybrids. Consequently, cavitation deformation predominated over shear yielding in hybrids.

1. Introduction

Polyamides (PA) are widely used engineering thermoplastics with easy processing and good mechanical properties. However, PA suffer from high moisture absorption and high notch sensitive characteristics. The shortcomings of polyamides can be overcome by blending with elastomers or with other polymers [1–5]. The impact modifiers commonly used in polyamides include ethylene propylene rubber [1], styrene-ethylene butylene-styrene (SEBS) or SEBS grafted with maleic anhydride (SEBS-g-MA) [2–4]. The cavitation of elastomer particles and associated matrix shear yielding are the main toughening mechanism for PA/elastomer blends. As the compatibility between PA and SEBS is relatively low, maleic anhydride (MA) is grafted to SEBS copolymer prior to blending with PA. The MA functional group of SEBS-g-MA can react with the amine and amide groups of PA, resulting in a finer dispersion of elastomers. Paul and coworkers reported that PA6,6 can be made super-tough by blending with SEBS-g-MA alone. They reported that melt blending of SEBS-g-MA with PA6,6 can produce the rubber particles within the optimal size range for effective toughening [3, 4]. The rubber toughening of polyamides is achieved at the expense of their stiffness and strength characteristics. The later deficiencies in rubber toughened polyamides can be restored by adding inorganic filler [6] or short glass fiber reinforcements [7–11], leading to the formation of ternary or hybrid composites.

For polymers in industrial applications, the fracture toughness of polymers is a critical factor in the materials selection. The toughness of materials is related to their deformation behavior and fracture mechanisms. The deformation mechanisms of polymers in the tensile process can be investigated by means of the tensile dilatometric technique. In the process, the volume change of samples during tensile process is determined. An increase in the volume strain is related to the cavitation-type deformation such as crazing, voiding

*Author to whom all correspondence should be addressed.

and debonding. Shear deformation generally produces no volume change. Many researchers have used tensile dilatometry to study the tensile deformation mechanisms of polymer blends and composites [12–26].

More recently, we have carried out a series of studies on the fabrication and the mechanical performance characteristics of short glass fiber (SGF) reinforced polypropylene hybrid composite toughened with SEBS or SEBS-g-MA [27–29]. The aims are directed towards basic understanding of the mechanisms related to the deformation, failure and toughening behavior of hybrid composites under tensile or impact loading. This work presents the results of investigation on the tensile deformation mechanism of SGF reinforced PA6,6 hybrid composite toughened with maleated SEBS.

2. Experimental

2.1. Materials

Polyamide 6,6 (Mitsubishi Engineering Plastics Co., Taiwan), SEBS-g-MA (Kraton FG 1901X; Shell Co.) and SGF with a length of ~4 mm (144A-14C; Owens Corning) were used in this work. The SGF was not treated with coupling agents. PA6,6 pellets and SGF were dried separately in ovens at 100°C for 48 h. SEBS-g-MA was dried at 60°C for 48 h.

2.2. Blending

The matrix of composites was PA6,6/SEBS-g-MA 80/20 (wt%) blend and designated as SGF0 in this article. The composites were reinforced with 5, 10, 15, 20 and 30 wt% SGF respectively (The glass fiber content was based on total mass of polymers). They were designated as SGF5, SGF10, SGF15, SGF 20 and SGF30, respectively. The composites were compounded in a Brabender twin-screw extruder. The dried polymer pellets and SGF were initially fed into a Brabender with operating temperature profiles of 260-270-270-260°C. The extruded strands were granulized with a pelletizer and dried. The dried pellets were fed into an injection molder (Cheng Hsong Jetmaster 4 Mark II-C) to produce plaques of 200 × 80 × 3.2 mm. Tensile specimens according to ASTM D368 were cut from the injection molded plaques.

2.3. Tensile dilatometry

Tensile dilatometric measurements of smooth specimens were carried out at room temperature (21°C) using a computer controlled Instron tensile tester (model 4206) under a crosshead speed of 1 mm/min. The relative humidity during the tests was 65%. In the tests, two extensometers were used to measure the longitudinal and transverse strains simultaneously. The transverse dimension could be width or thickness, but only the width displacement was determined. The gauge lengths of the longitudinal and transverse extensometers were 12.5 mm and 15 mm, respectively. The thickness strain and the width strain were assumed to be equal. To avoid damage to the extensometers during tensile tests, the experiments were terminated after reaching the maximum yield stress and prior to necking.

2.4. SEM examination

Small block specimens were cut from central gauge length region after dilatometric test. The blocks were then notched and sharpened with a sharp razor blade. They were immersed in liquid nitrogen for about 15 min. Thereafter, the blocks were removed from the liquid nitrogen and immediately fractured along the tensile direction by tapping with sharp wedge into the notches [24]. The fracture surfaces were coated with a thin layer of gold prior to examination in a scanning electron microscope (JEOL JSM 820 SEM).

3. Results and discussion

3.1. Dilatational response

According to the literature [30, 31], an increase in the volume strain of the bulk solid associated with the application of a tensile stress can be expressed as follows,

$$\frac{\Delta V}{V} = (1+\varepsilon_l)(1+\varepsilon_w)(1+\varepsilon_t) - 1 \qquad (1)$$

Where ΔV is the change in volume; V is the original volume; the ratio $\Delta V/V$ is the volume strain; and ε_l, ε_w and ε_t are the longitudinal, transverse, and thickness engineering strains respectively. For isotropic material, the fundamental elastic constants such as modulus, E, and lateral contraction ratio, ν, are direction independent. Accordingly, the lateral contraction ratios in the width and thickness directions are equivalent [22],

$$\nu = -\frac{\varepsilon_w}{\varepsilon_l} = -\frac{\varepsilon_t}{\varepsilon_l} \qquad (2)$$

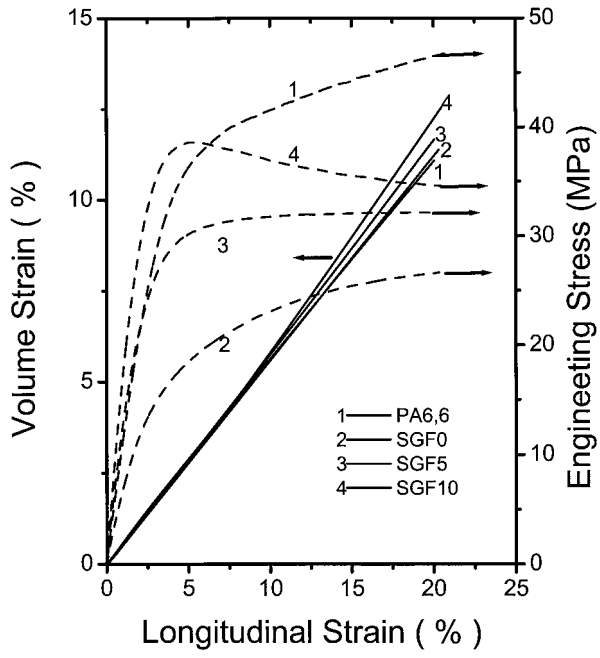

Figure 1 Engineering stress and volume strain versus longitudinal strain curves for PA6,6 polymer, SGF0 blend, SGF5 and SGF10 hybrids. Full-line curves correspond to the plots of volume strain vs longitudinal strain. Dash-line curves correspond to the plots of engineering stress vs. longitudinal strain.

Equation 1 then reduces to:

$$\frac{\Delta V}{V} = (1 + \varepsilon_l)(1 + \varepsilon_t)^2 - 1 \qquad (3)$$

Fig. 1 shows the engineering stress and volume strain versus longitudinal strain curves for the PA6,6 polymer, SGF0 blend, and hybrids reinforced with low volume content of SGF. Pure PA6,6 polymer and SGF0 blend exhibit typical ductile behavior during tensile deformation. The incorporation of SEBS-g-MA leads to a decrease in yield stress as expected. The yield stress is effectively restored by adding 10% SGF. It can be seen from Fig. 1 that the volume strains for these samples increase linearly with increasing longitudinal elongation. The volume strain of SGF0 blend containing maleated SEBS elastomer is slightly larger than that for PA6,6. This is because the elastomer particles can act as stress concentrators, initiating crazes in the matrix near the periphery of particles and producing cavitation. Incorporation of low SGF content leads to the volume strains of hybrids become higher than that of the SGF0 blend. Fig. 2 shows the engineering stress and volume strain versus longitudinal strain curves for the SGF15, SGF20 and SGF30 hybrids. The yield stress of hybrid appears

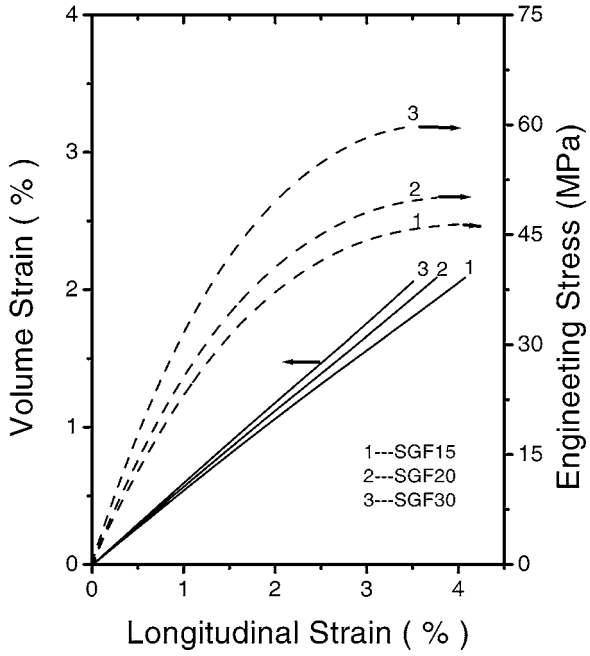

Figure 2 Engineering stress and volume strain versus longitudinal strain curves for the SGF 15, SGF 20 and SGF 30 hybrid composites. Full-line curves correspond to the plots of volume strain vs longitudinal strain. Dash-line curves correspond to the plots of engineering stress vs. longitudinal strain.

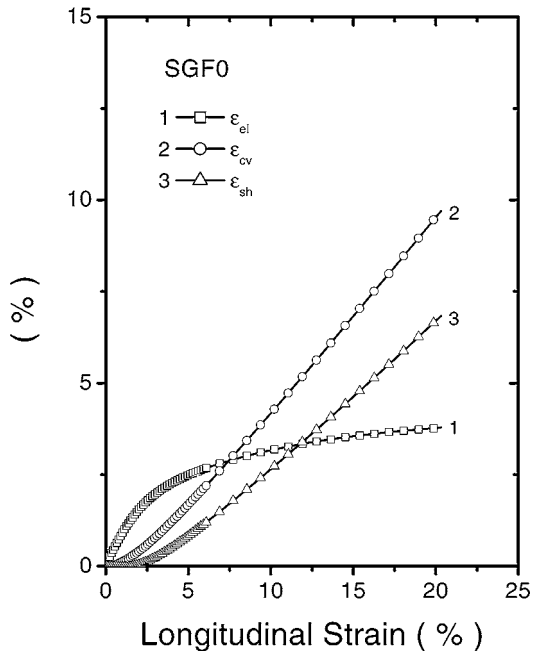

Figure 3 Plots of the elongation strains caused by elastic deformation (ε_{el}), cavitation (ε_{cv}) and shear deformation (ε_{sh}) versus the total elongation strain for SGF0 blend.

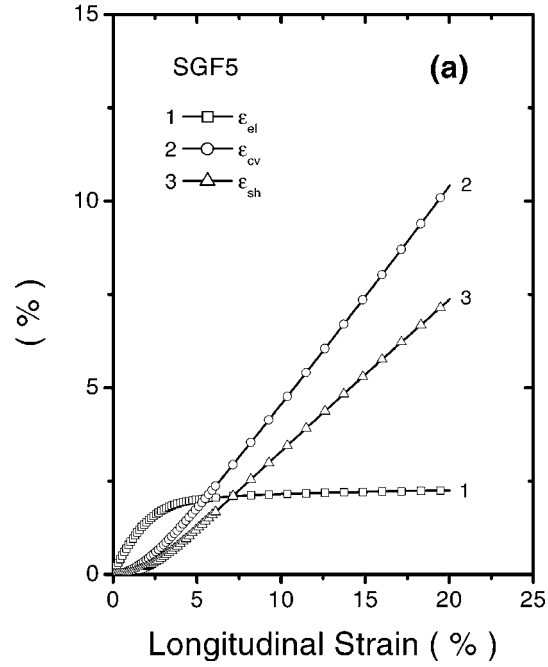

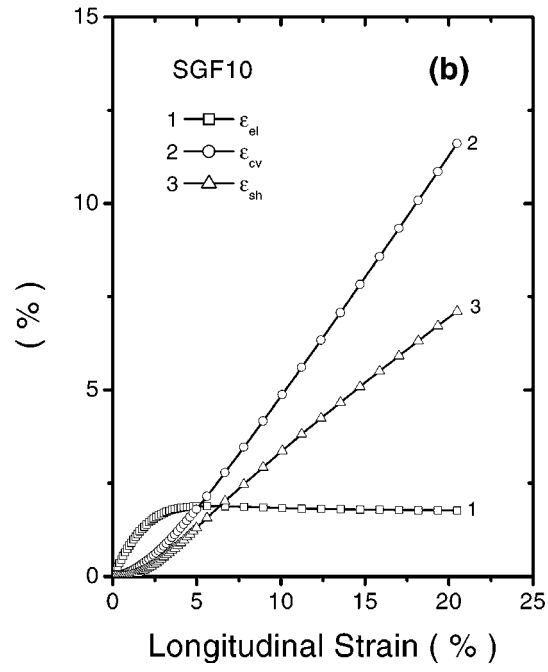

Figure 4 Plots of the elongation strains caused by elastic deformation (ε_{el}), cavitation (ε_{cv}) and shear deformation (ε_{sh}) versus the total elongation strain for (a) SGF5 and (b) SGF10 hybrids.

to increase with increasing SGF content. It is also apparent that the volume change versus longitudinal strain is linear for these hybrid composites. Naqui *et al*. indicated that an applied stress within a small deformation limit can be analyzed in terms of normal hydrostatic and deviatioric components [22] The hydrostatic stress yields an increase in the volume in the dilatational response of the material, while the deviatioric (shear) stress results in a change of shape, not volume.

Heikens *et al*. have proposed a quantitative model to take into accounts the contributions of various deformations (i.e., elastic, shear, and cavitation) to the total longitudinal elongation [30, 31]. In this model, the respective contributions of elastic deformation, shear deformation, and cavitation to the total elongation strain and the total volume strain are assumed to be additive. The cavitation includes all deformation processes that lead to an increase in volume strain, such as crazing, cavitation of rubber particles, debonding of reinforcing filler at the interfaces etc. And the volume strain caused by cavitation is assumed to be equal to the elongation strain. In contrast, shear deformation makes a negligible contribution to the volume strain. It must be pointed out that the important criteria for use of this model is that the specimen must elongate uniformly throughout the entire gauge portion [30, 31]. This means that this model may only be applied to the polymer specimens prior to necking.

According to this model, at any elongation strain, the strains caused by elastic deformation (ε_{el}), shear deformation (ε_{sh}), and cavitation deformation (ε_{ca}) can be calculated from σ_T-ε-$\Delta V/V$ diagrams and are given

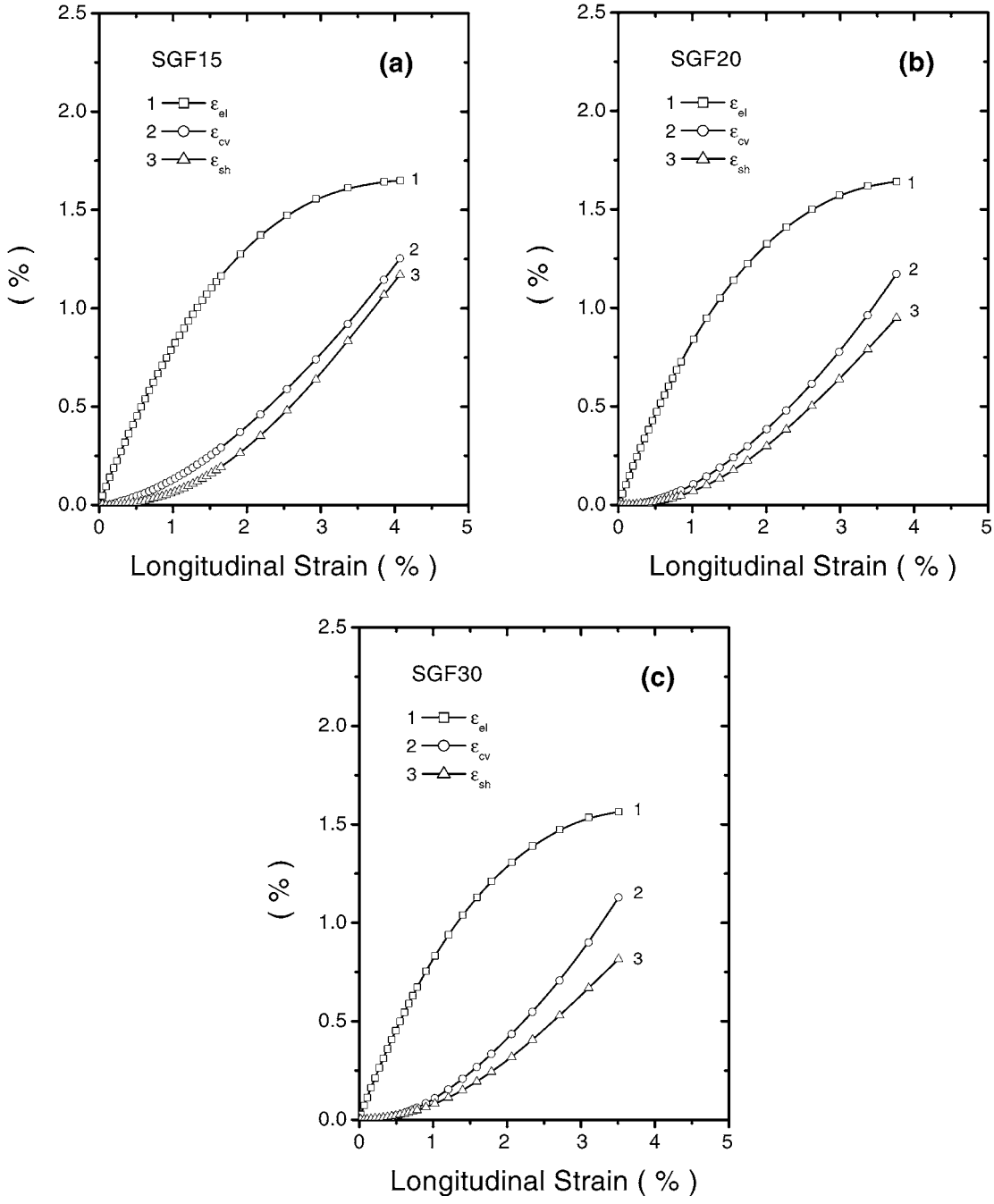

Figure 5 Plots of the elongation strains caused by elastic deformation (ε_{el}), cavitation (ε_{cv}) and shear deformation (ε_{sh}) versus the total elongation strain for (a) SGF15, (b) SGF20 and (c) SGF30 hybrids.

by the following equations:

$$\varepsilon_{el} = \frac{\sigma_T}{E} \tag{4}$$

$$\varepsilon_{cv} = \frac{\Delta V}{V} - \frac{(1-2\nu)\sigma_T}{E} \tag{5}$$

$$\varepsilon_{sh} = \varepsilon - \frac{\Delta V}{V} - \frac{2\nu\sigma_T}{E} \tag{6}$$

where σ_T is the true stress, E is young's modulus, ε is the elongation strain, and ν is the Poisson's ratio. The E and ν can be determined from the initial slopes of σ_{eng}-ε (σ_{eng} is the engineering stress) and ε_t-ε curves, respectively. The true stress is calculated using the instantaneous cross-sectional area over which the deformation occurs. The relation between the true and engineering stress is

$$\sigma_T = \frac{\sigma_{eng}}{(1-\varepsilon_t)^2} \tag{7}$$

The elongation strains caused by the elastic deformation, shear deformation and cavitation process as a function of the total longitudinal strain for the SGF0 blend are shown in Fig. 3. It is apparent that the elastic deformation controls in low strain regime. Thereafter, cavitation is the dominant deformation mode at high strain region. And cavitation strain observed in the SGF0 blend is believed to be associated with the cavitation of rubber particles from the PA6,6 matrix. Fig. 4a and b shows the separate contributions of the three different deformations during the tensile process for hybrids reinforced with low SGF content. Similar strain characteristics are observed but the cavitation strain appears to increase with the incorporation of glass fibers.

Fig. 5a–c shows the plots of elongation strains due to elastic deformation, shear deformation, and cavitation deformation versus the total elongation strain for the SGF15, SGF20 and SGF30 hybrids, respectively. Fig. 5a reveals that the elastic deformation is the dominant deformation over the total strain range studied. The shearing and cavitation deformation strains are much smaller compares to the elastic strain. The cavitation deformation obviously predominates over the shear deformation at higher strain region. The cavitation strain in these hybrids arises from weak interfacial bonding between the SGF and the matrix. When the hybrid samples are stressed in uniaxial tension, debonding between the SGF and matrix occurs readily, leading to the formation of voids.

We now consider the interfacial bonding developed between various phase components of PA6,6 hybrids. The interactions consist of the interfacial bonding between the matrix (PA6,6) and SEBS, between the SEBS and SGF, and between the PA6,6 and SGF. For the matrix polymers, the MA functional group grafted to the central EB chain segment of SEBS copolymer can react with the amine and amide groups of PA6,6. And the reaction between anhydride and amine end group yields an imide linkage. The graft polymer at interface lowers the interfacial tension, and stabilizes the dispersion against coalescence, leading to a fine dispersion. Paul and coworkers reported PA6,6 is bifunctional, i.e. there are sometimes two amine end groups in one chain whilst PA6 is monofunctional to anhydrides. PA6 can be toughened by blending with appropriate combination of SEBS and SEBS-g-MA. This is because pure SEBS particles are too large for toughening PA6, whereas SEBS-g-Ma particles are too small for optimal toughening. In contrast, PA6,6 can be toughened by blending with SEBS-g-MA alone, and addition of SEBS merely reduced toughness [2, 3].

In general, anhydride functional group grafted to EB can react with hydroxyl groups on the glass fiber surfaces during compounding, thereby improving the compatibility between the SGF and SEBS. The reaction

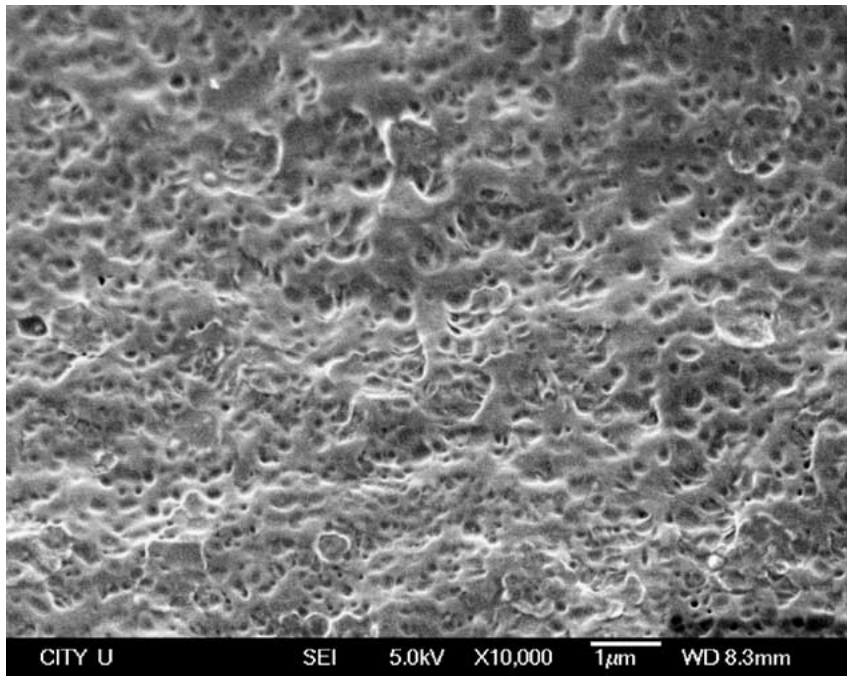

Figure 6 SEM micrograph showing the fracture morphology of the SGF0 blend subjected to dilatometric test.

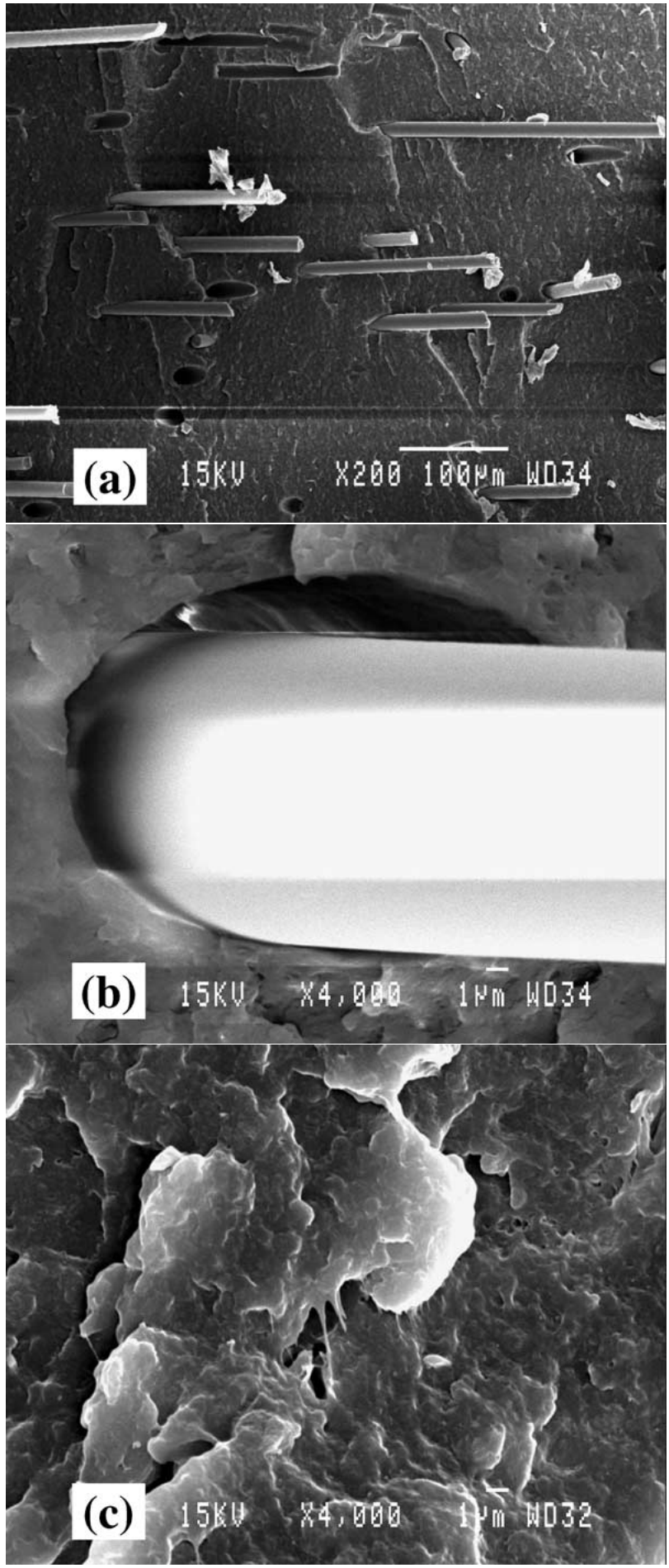

Figure 7 SEM micrographs showing the fracture morphologies the SGF5 hybrid subjected to dilatometric test. (a) Low magnification fractograph; (b) Higher magnification view showing formation of voids at the glass-fiber interface associated with debonding and pull-out of fibers; (c) Higher magnification view showing crazes in the matrix of hybrid.

takes place between SEBS-g-MA and SGF is shown as follows,

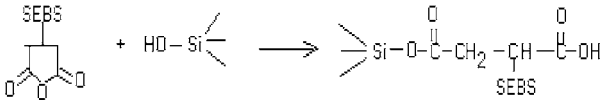

As discussed above, most of MA functional group of SEBS can react readily with the amine and amide groups of PA6,6. Consequently, only fewer remaining MA groups are available to react with the hydroxyl groups on the SGF surfaces. The interaction between the maleated SEBS and SGF is weakened accordingly, leading to the microvoiding and debonding of SGF from the matrix. In the case of PA6,6 and SGF interaction, only weak physical interaction can develop between them due to their polar structures.

3.2. Fractography

Fractogtaphy can provide information on the failure mode such as cavitation, shear yielding and debonding of SGF at the matrix/fiber interface. Fig. 6 shows the SEM fractograph of the SGF0 blend subjected to dilatometric test. This micrograph shows the presence of microvoids resulting from cavitation of the rubber particles dispersed in the PA6,6 matrix during tensile deformation. Elastomer cavitation then triggers shear yielding of the matrix, and this induces the shear strain as shown in Fig. 3. Fig. 7a–c shows the SEM fractographs of the SGF5 hybrid deformed in uniaxial tension. Debonding and pull-out of fibers are evident in the fractographs. Moreover, crazes are also evident in some areas of the matrix. The debonding voids and crazes contribute to the cavitation strain as depicted in Fig. 4a. And the cavitation predominates over shear yielding.

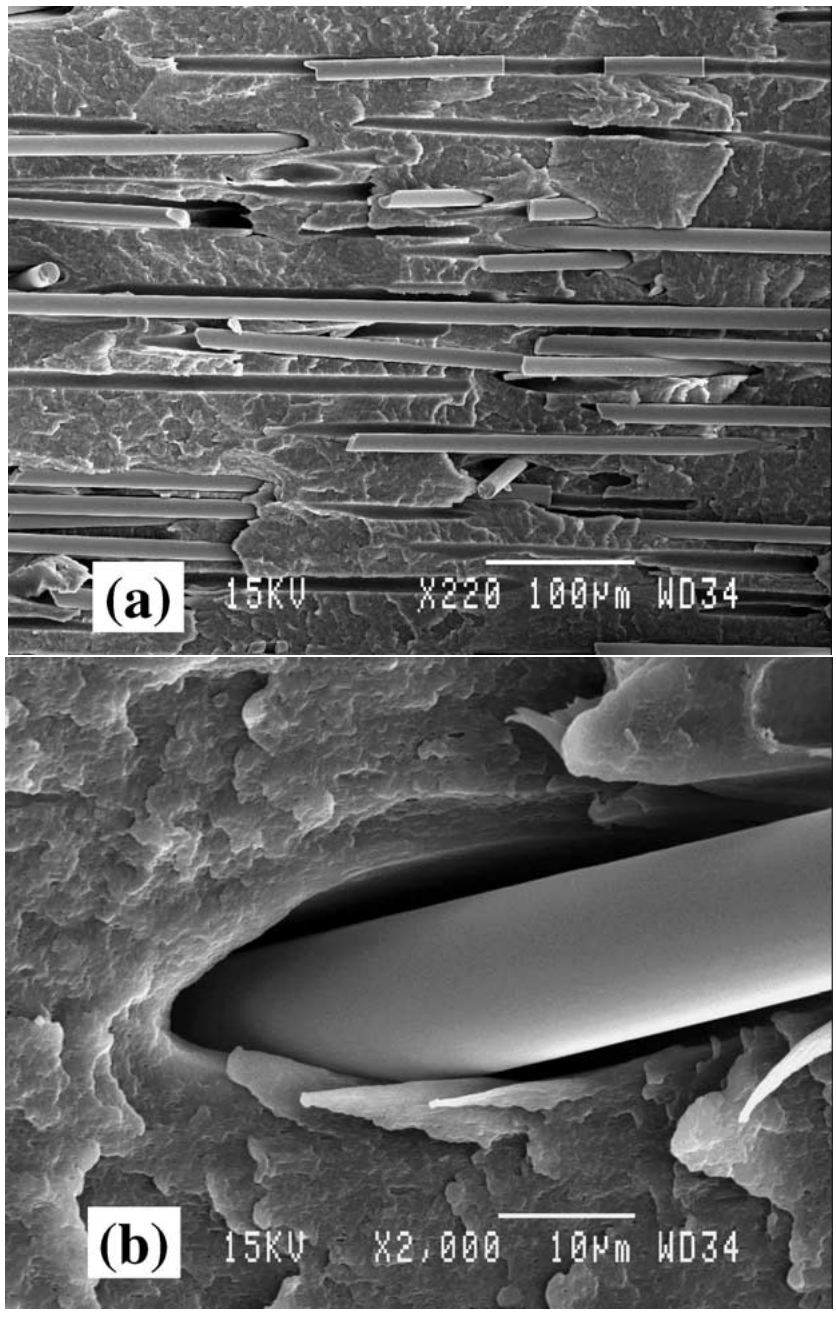

Figure 8 SEM micrographs showing the fracture morphologies the SGF15 hybrid subjected to dilatometric test. (a) Low magnification fractograph; (b) Higher magnification view showing formation of microvoids at the glass-fiber interface.

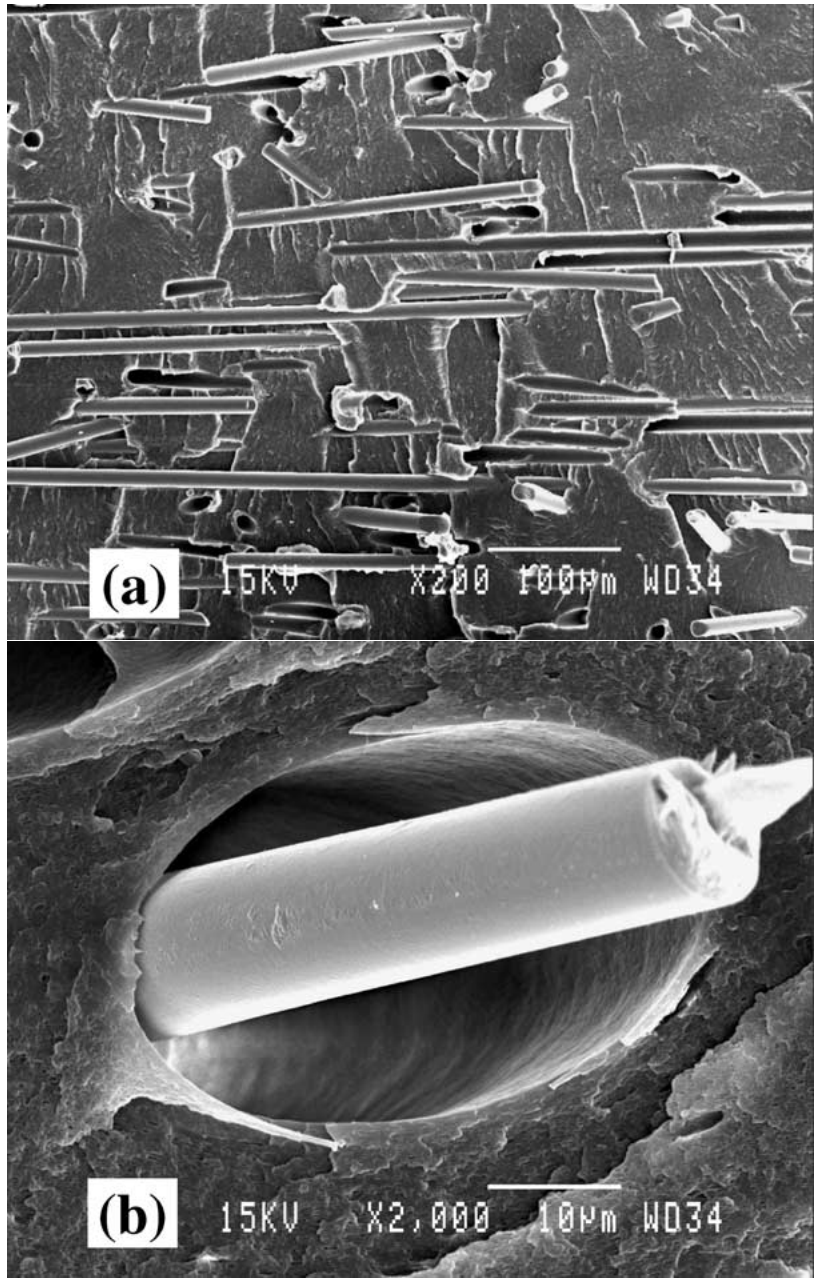

Figure 9 SEM micrographs of the SGF30 hybrid subjected to dilatometric test showing (a) Low magnification fractograph; (b) Higher magnification view showing formation of microvoids at the glass-fiber interface.

With further increasing the SGF content, microvoids due to the debonding of glass fiber can be readily seen (Figs 8 and 9). From the basis of the above observation, we conclude that glass fiber debonding and pull-out are the main energy dissipation mechanisms for the PA6,6 hybrids during tensile deformation.

4. Conclusions

Tensile dilatometry is a potential technique to characterize the deformation mechanisms of ductile SGF0 blend and its hybrid composites. The measurements indicate that both cavitation and shear yielding occur in SGF0 blend during deformation. But the cavitation deformation prevails over shear yielding in the SGF0 blend after the initial elastic deformation. Dilatational response of this blend is derived from the cavitation of rubber particles dispersed in PA6,6 matrix. In contrast, voids originate from the debonding of glass fiber from PA6,6 matrix contribute to the cavitation strain in the hybrids. Consequently, cavitation predominates over shearing deformation. Finally, the elastic deformation is the dominant deformation mechanism for the hybrids reinforced with higher SGF content. SEM fractographic analyses generally correlate well with tensile dilatometric results.

Acknowledgment

The work described in this paper was fully supported by a grant from the Research Grants Council of Hong Kong Special Administrative Region, China (Project no. CityU 1029/00E).

References

1. K. DIJKSTRA, J. TER LAAK and R. J. GAYMANS, *Polymer* **35** (1994) 315.
2. A. J. OSHINSKI, H. KEKSKULA and D. R. PAUL, *ibid.* **33** (1992) 268.
3. *Idem.*, *ibid.* **33** (1992) 284.

4. Y. TAKEDA, H. KEKSKULA and D. R. PAUL, *ibid.* **33** (1992) 3173.
5. S. C. WONG and Y. W. MAI, *ibid.* **40** (1999) 1553.
6. S. C. TJONG and S. A. XU, *J. Appl. Polym. Sci.* **81** (2001) 3231.
7. T. J. PECORINI and R. W. HERTZBERG, *Polym. Compos.* **15** (1994) 174.
8. M. L. SHIAO, S. V. NAIR, P. D. GARRETT and R. E. POLLARD, *Polymer* **35** (1994) 306.
9. S. V. NAIR, A. SUBRAMANIAM and L. A. GOETTLER, *J. Mater. Sci.* **32** (1997) 5335.
10. *Idem.*, *ibid.* **32** (1997) 5347.
11. *Idem.*, *ibid.* **33** (1998) 3455.
12. M. E. J. DEKKERS and D. J. HEIKENS, *J. Appl. Polym. Sci.* **30** (1985) 2389.
13. *Idem.*, *J. Mater. Sci.* **20** (1985) 3873.
14. M. E. J. DEKKERS, S. Y. HOBBS and V. H. WATKINS, *ibid.* **23** (1988) 1225.
15. S. Y. HOBBS and M. E. J. DEKKERS, *ibid.* **24** (1989) 1316.
16. C. B. BUCKNALL, D. CLAYTON and W. J. KEAST, *ibid.* **8** (1973) 514.
17. C. B. BUCKNALL and W. W. STEVENS, *ibid.* **5** (1980) 2950.
18. C. B. BUCKNALL and C. J. PAGE, *ibid.* **17** (1982) 808.
19. C. B. BUCKNALL, D. CLAYTON and W. J. KEAST, *ibid.* **19** (1984) 2064.
20. C. B. BUCKNALL, P. DAVIES and J. K. PARTRIDGE, *ibid.* **21** (1986) 307.
21. C. B. BUCKNALL, P. S. HEATHER and A. J. LAZZERI, *ibid.* **24** (1989) 2255.
22. S. I. NAQUI and I. M. ROBINSON, *ibid.* **28** (1993) 1421.
23. J. M. C. SCHWARZ, H. KESKKULA, J. W. BARLOW and D. R. PAUL, *J. Appl. Polym. Sci.* **35** (1988) 653.
24. A. GONZALEZ-MONTIAL, H. KESKKULA and D. R. PAUL, *Polymer* **36** (1995) 4621.
25. S. A. XU and C. M. CHAN, *Polymer J.* **30** (1998) 552.
26. S. A. XU and S. C. TJONG, *J. Appl. Polym. Sci.* **77** (1999) 2024.
27. S. C. TJONG, S. A. XU, R. K. Y. LI and Y. W. MAI, *Compos. Sci. Technol.* **62** (2002) 831.
28. *Idem.*, *Polym. Int.*, in-press.
29. *Idem.*, *J. Appl. Polym. Sci.* **86** (2002) 1303.
30. D. HEIKENS, S. D. SJOERDSMA and W. J. COUMANS, *J. Mater. Sci.* **8** (1973) 514.
31. *Idem.*, *ibid.* **16** (1981) 429.

Received 19 May
and accepted 20 August 2002